Object-Based Change Detection for VHR Images Based on Multiscale Uncertainty Analysis

Article *in* IEEE Geoscience and Remote Sensing Letters · December 2017
DOI: 10.1109/LGRS.2017.2763182

3 authors:

Yongjun Zhang
Wuhan University
112 PUBLICATIONS **665** CITATIONS
SEE PROFILE

Daifeng Peng
Wuhan University
6 PUBLICATIONS **7** CITATIONS
SEE PROFILE

Xu Huang
Wuhan University
28 PUBLICATIONS **173** CITATIONS
SEE PROFILE

Object-Based Change Detection for VHR Images Based on Multiscale Uncertainty Analysis

Yongjun Zhang, Daifeng Peng, and Xu Huang

***Abstract*— Scale is of great significance in image analysis and interpretation. In order to utilize scale information, multiscale fusion is usually employed to combine change detection (CD) results from different scales. However, CD results from different scales are usually treated independently, which ignores the scale contextual information. To overcome this drawback, this letter introduces a novel object-based change detection (OBCD) technique for unsupervised CD in very high-resolution (VHR) images by incorporating multiscale uncertainty analysis. First, two temporal images are stacked and segmented using a series of optimal segmentation scales ranging from coarse to fine. Second, an initial CD result is obtained by fusing the pixel-based CD result and OBCD result based on Dempter–Shafer (DS) evidence theory. Third, multiscale uncertainty analysis is implemented from coarse scale to fine scale by support vector machine classification. Finally, a CD map is generated by combining all the available information in all the scales. The experimental results employing SPOT5 and GF-1 images demonstrate the effectiveness and superiority of the proposed approach.**

***Index Terms*— Change detection (CD), Dempter–Shafer (DS) evidence theory, multiscale, support vector machine (SVM), uncertainty analysis.**

I. Introduction

CHANGE detection (CD) is the process of identifying the difference in the state of an object or natural phenomena by observing it at different times [1]. Remote-sensing imagery is widely used in CD research, where the coverage areas are large, the revisit times are short, and the image information is abundant. CD has become an increasingly popular research topic due to its important practical applications, such as land cover transitions, resources investigation, urban expansion monitoring, and disaster assessment [2]. During the past decades, numerous CD methods have been proposed, and the investigations conducted mainly can be divided into pixel-based and object-based methods in terms of their basic unit for image analysis.

In the pixel-based case, the change features from two images are compared for each pixel independently, whereas in the object-based case, the images are segmented into disjoint and homogeneous objects. The object features are then extracted and compared for change analysis. Pixel-based CD (PBCD) methods are mainly employed in medium- and low-resolution remote sensing imagery, which mainly consists of two steps: 1) generating the difference image pixel by pixel and 2) obtaining the change map by analyzing it. Many PBCD techniques have been developed, including change vector analysis (CVA) [3], principal component analysis (PCA) [4], postclassification [5], and machine learning [6]. However, contextual information is neglected in PBCD methods, leading to lower CD accuracy and "salt and pepper" noise. To overcome these drawbacks, a number of techniques have been developed to integrate spatial-context information, including neighboring windows [7], level set [8], hypergraph [9], Markov random field and conditional random field [10].

With the ever-increasing availability of VHR images, the capability of PBCD methods has become limited due to its assumption of spatial independence among pixels, while object-based change detection (OBCD) has become increasingly popular as it can properly exploit the specific properties of VHR images and detect changes at a more detailed spatial scale [11]. In OBCD, the object is the basic analysis unit, which contains rich information, including spectrum, texture, shape, and spatial context, making it easy to delineate the objects and to model the contextual information comprehensively. Generally, three main OBCD methods can be categorized as follows: 1) feature-based CD (FOCD); 2) classification-based CD (COCD); and 3) hybrid CD (HCD). In FOCD, the change map is generated by the similarity analysis of the feature vectors of the segmented objects [12], [13]; while the comparison and analysis of the geometry and class membership of the objects are employed to generate the change map in COCD [14], [15]. The HCD approach makes full use of the classification and feature extraction techniques for specific object CD [16].

However, only single-scale information is utilized to model the images within all the OBCD methods above. In the literature, some attempts have been made to model image information at different scales. Bovolo [17] proposed a multilevel parcel-based approach, where the CD map is achieved by applying a multilevel CVA analysis to each pixel. In [18] and [19], based on the initial CD results from different scales ranging from coarse to fine, the final CD map was generated by multiscale fusion. However, there still exist limitations within the above methods, where CD results from different scales are treated independently. As the uncertain CD map generated in the coarse scale could be refined in the fine scale, further investigation is needed so as to make full use of CD results from different scales.

To address the aforementioned problems, this letter introduces a novel OBCD method based on multiscale uncertainty

Manuscript received August 1, 2017; revised September 12, 2017; accepted October 9, 2017. Date of publication December 13, 2017; date of current version December 27, 2017. This work was supported by the National Natural Science Foundation of China under Grant 41571434, Grant 41322010, and Grant 41701540.

Y. Zhang and D. Peng are with the School of Remote Sensing and Information Engineering, Wuhan University, Wuhan 430079, China (e-mail: zhangyj@whu.edu.cn; daifeng@whu.edu.cn).

X. Huang is with the Information Technology Research Department, Wuhan Engineering Science and Technology Institute, Wuhan 430019, China (e-mail: huangxurs@whu.edu.cn).

Color versions of one or more of the figures in this letter are available online at http://ieeexplore.ieee.org.

Digital Object Identifier 10.1109/LGRS.2017.2763182

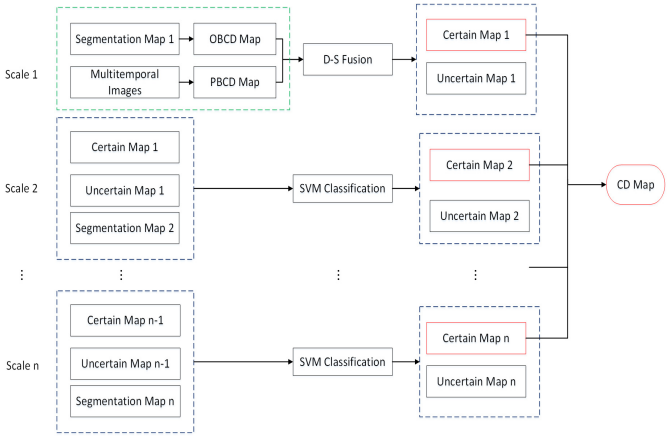

Fig. 1. Framework of the proposed CD approach.

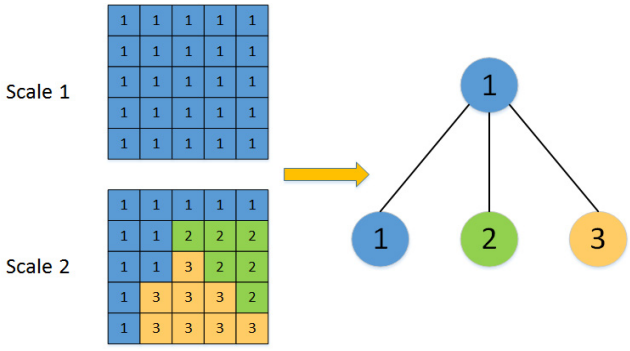

Fig. 2. Illustration of father–child relationship between scales.

analysis (OB-MSUA) for CD in VHR images, where the optimal segmentation scales are chosen for generating the corresponding segmentation maps. D-S evidence theory and support vector machine (SVM) are then utilized for uncertainty analysis between the CD results from different scales. The main contributions of the proposed approach are twofold: 1) scale constraints are constructed between neighboring scales so that multiscale context-based image information can be utilized and 2) SVM classification is utilized for multiscale uncertainty analysis, where the current-scale and upper scale image information are fully considered.

The remainder of this letter is organized as follows. Section II describes the proposed CD approach in detail. Section III presents experiments and analysis; and finally, the conclusions of this letter are presented in Section IV.

II. Proposed Approach

"From coarse to fine, refine layer by layer" is a classical strategy in the field of pyramid image matching. Inspired by that method, we implemented the multiscale uncertainty analysis into OBCD. As shown in Fig. 1, the proposed approach consists of the following steps.

1) Based on optimal scales, multitemporal images are segmented to generate a set of segmentation maps ranging from fine scale to coarse scale.
2) The CD process starts at the coarsest scale, where both the PBCD map and the OBCD map are generated for D-S evidence theory fusion, and a certain CD map and an uncertain CD map are then obtained through uncertainty analysis.
3) The uncertainty analysis results are projected onto the fine scale segmentation map, where the certain CD objects are treated as the training samples for the SVM classifier and the uncertain CD objects are then classified using the trained SVM classifier, so as to generate new certain and uncertain CD maps based on the probabilistic output of the SVM.
4) Step 3) is repeated until all the uncertain objects are refined to certain objects, whereby the uncertain CD results are refined on a finer scale layer by layer.
5) The final CD map is generated by searching all the certain maps from the different scales. Further details about the proposed approach are presented in Sections II-A–II-C.

A. Multitemporal Images Segmentation and Scale Constraints Building

1) Multitemporal Images Segmentation: Image segmentation is the basis and core of object-based image analysis, where the scale parameter is of great significance to improving segmentation performance. VHR images, due to the complexity of the scenes, often contain various kinds of ground objects, each of which corresponds to an optimal expression scale. Thus, a series of segmentation scales needs to be set for better delineation of different ground objects. In this letter, multiresolution segmentation (MRS), which is embedded in eCognition software, is utilized for image segmentation [20]; a global score (GS) [21] is employed for computing a series of optimal scales for different ground objects.

2) Scale Constraints Building: In MRS, multiscale segmentation results are obtained through region merging, where a series of scale thresholds are set. The region merging process stops when the heterogeneity between neighboring objects exceeds the threshold.

The remarkable advantage of the aforementioned region merging is that the object boundaries in the upper scale are determined by the object boundaries in the lower scale, which means that a simple father–child relationship can be built between the scales. For example, object 1 in scale 1 can be regarded as the father of objects 1–3 in scale 2; and objects 1–3 in scale 2 can be seen as the children of object 1 in scale 1 (see Fig. 2).

Generally, multiscale segmentation results are stored in the form of a label matrix, where the elements of each object are assigned a unique label value. Therefore, the father–child relationship of objects between neighboring scales can be constructed by the label mapping relationship in the label matrix, as shown in Fig. 2, from which the scale constraints can thus be built.

B. Initial Change Information Generation

Considering two multispectral images X_1 and X_2 of size $M \times N$ with B bands acquired over the same geographical area at two different times, suppose that such images have been well preprocessed, including radiometric calibration and coregistration. Let X_i^b $(i = 1, 2)$ be the values of $M \times N$ pixels in the bth $(1 \le b \le B)$ band of X_i, and difference image X_D can be defined as

$$X_D = \sqrt{\sum_{b=1}^{B} \left(X_1^b - X_2^b\right)^2}. \quad (1)$$

1) PBCD and OBCD Map Generation: PBCD results can be obtained by threshold segmentation of the difference image X_D. For all the pixels $X_{Dk}(1 \le k \le M \times N)$ in the difference image, two categories can be divided: the changed class and the unchanged class. The pixel values of the changed class are large, while those in the unchanged class are small. In this letter, all the pixels in X_D are assumed to be a Gaussian mixture distribution composed of two Gaussian components, which are defined as follows:

$$p(X_{Dk}) = p(\omega_c)p(X_{Dk}|\omega_c) + p(\omega_n)p(X_{Dk}|\omega_n) \tag{2}$$

$$p(X_{Dk}|\omega) = \frac{1}{\sqrt{2\pi}\delta_\omega}\exp\left(-\frac{(X_{Dk}-\mu_w)^2}{2\delta_\omega^2}\right) \quad \omega \in \{\omega_c, \omega_n\} \tag{3}$$

where ω_c and ω_n represent the class of the changed and unchanged pixels, respectively. $p(\omega_c)$ and $p(\omega_n)$ denote the corresponding proportions pixels, and $p(\omega_c) + p(\omega_n) = 1$. μ_ω is the mean value of the pixels, and δ_ω is the standard deviation of the pixels. An expectation maximization (EM) algorithm is then employed to estimate the parameters of the Gaussian mixture distribution, and a reasonable threshold is determined for classifying the pixels into "changed" and "no-changed" based on the pixel values [3].

Supposing that the number of objects in the coarsest scale is K, for each object $R_i(1 \le i \le K)$, the spectral histograms in two temporal images are calculated. Let h_1 and h_2 be the two periods of histograms, L the quantization level of the histograms, and $f_i^b(1 \le i \le L, 1 \le b \le B)$ the frequency of gray level i of the histograms on band b. The heterogeneity of the objects is calculated by their histogram distance

$$H_{R_i} = \frac{1}{B}\sum_{b=1}^{B} G^b(h_1, h_2) \tag{4}$$

where $G^b(h_1, h_2)$ denotes the histogram distance calculated by the G statistic [22]. All the values of object heterogeneity make up the set $H = \{H_{R_1} \ldots, H_{R_i} \ldots, H_{R_K}\}$, and H_{R_i} represents the heterogeneity of the ith object. In order to obtain the probability output of the each object belonging to the changed class or unchanged class, the fuzzy c-means (FCM) algorithm [23] is then employed on set H.

2) CD Results Fusing Using D-S Evidence Theory: In order to make full use of the advantages of PBCD and OBCD, D-S evidence theory is employed. In D-S evidence theory [24], let Θ be the frame of discernment, then the power set of Θ is denoted by 2^Θ. A probability mass, $m(A)$, is assigned to every class $A \in 2^\Theta$ by a source, such that $0 \le m(A) \le 1, m(\emptyset) = 0$, and $\sum_{A \in 2^\Theta} m(A) = 1$, where $\emptyset$ denotes the empty set.

D-S evidence theory combines the different evidences with an orthogonal sum. If p sources are available and m_1, m_2, $m_3, \ldots, m_p$ are assumed to be the corresponding probability masses, their orthogonal sum is denoted as

$$m = m_1 \oplus m_2 \oplus \cdots \oplus m_p \tag{5}$$

and the combined mass for each class $A \in 2^\Theta$ is defined as follows:

$$m(A) = \frac{\sum_{\cap A_i = A}\prod_{1 \le j \le p} m_j(A_i)}{1 - \sum_{\cap A_i = \phi}\prod_{1 \le j \le p} m_j(A_i)}. \tag{6}$$

In this letter, the discernment frame $\Theta = \{C, U\}$, where C represents the changed class and U is the unchanged class. Two evidences are generated and combined in this letter: PBCD and OBCD. Let m_1 be the evidence obtained from PBCD, for object $R_i(1 \le i \le K)$, and the evidence $m_1 = \{P_{1c}, P_{1u}\}$ is defined as follows:

$$\begin{cases} P_{1c} = \dfrac{n_c}{n} \\ P_{1u} = \dfrac{n_u}{n} \end{cases} \tag{7}$$

where P_{1c} and P_{1u} represent the probability of object R_i belonging to C and U, respectively, in PBCD, n_c and n_u are the number of pixels in object R_i belonging to C and U, respectively, and n is the total number of pixels in object R_i.

Assuming m_2 is the evidence obtained from OBCD, for object $R_i(1 \le i \le K)$, the evidence $m_2 = \{P_{2c}, P_{2u}\}$ is defined as follows:

$$\begin{cases} P_{2c} = p_c(R_i) \\ P_{2u} = p_u(R_i) \end{cases} \tag{8}$$

where P_{2c} and P_{2u} represent the probability of object R_i belonging to C and U, respectively, in OBCD, and $p_c(R_i)$ and $p_u(R_i)$ denote the probability of object R_i belonging to C and U by the FCM algorithm.

Then m_1 and m_2 are combined using (6) to generate new evidence $m = \{P_c, P_u\}$, where P_c and P_u represent the probability of object R_i belonging to C and U, respectively, in m.

Based on P_c and P_u, a threshold T is then set to classify the objects into the changed, unchanged, and uncertain classes with the following formula:

$$l_i = \begin{cases} 0 & \text{if } T > P_c \\ 1 & \text{if } T > P_u \\ 2 & \text{else.} \end{cases} \tag{9}$$

C. Multiscale Uncertainty Analysis

In order to determine the change type of the uncertain class in the coarsest scale, both certain and uncertain maps are projected onto a finer scale to generate the initial changed, unchanged and uncertain classes. SVM is employed, where the changed class and the unchanged class serve as the training samples and the uncertain class serves as the testing samples. Both the mean values in the difference images and the heterogeneity calculated by the G-statistic are used as input features for the SVM classifier. Based on the probability output of the SVM classifier, uncertainty analysis is implemented using (9), thus certain and uncertain maps can be generated. Then, both certain and uncertain maps are projected onto a finer scale so that the uncertain class is further analyzed as shown above, which iterates until no uncertain class exists or the finest segmentation map has been utilized. Through the above process, the uncertain information in the initial CD map is refined layer by layer, and the final CD map is generated by combining all the certain maps.

III. Experiments and Analysis

A. Data Sets Description and Experimental Settings

To evaluate the performance of the proposed approach, two multi-temporal VHR remote sensing image data sets from optical satellites were used. The first data set (DS1) contained two periods of Systeme Probatoire d'Observation

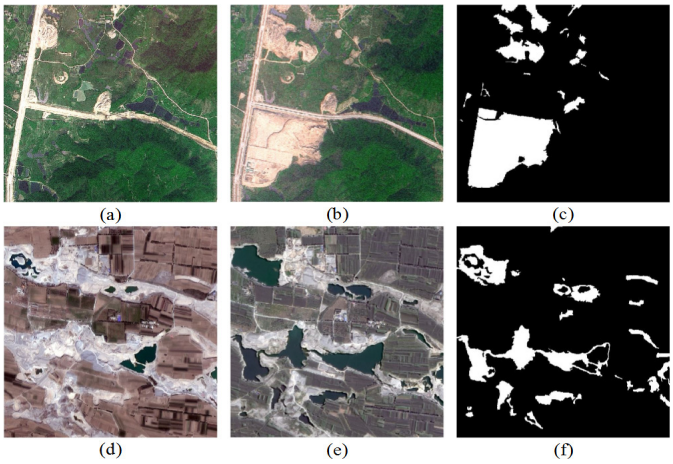

Fig. 3. Illustration of two data sets. (a)–(c) Input multitemporal images and reference change map of DS1, respectively. (d)–(f) Input multitemporal images and reference change map of DS2, respectively. The changes are marked in white for each reference change map.

de la Terre 5 (SPOT-5) multispectral images comprised of three bands of red, green, and near infrared with a spatial resolution of 2.5 m, acquired over the region of Guangzhou City, China in October 2006 and again in October 2007. The region is an 877 × 738 pixels area containing vegetation, bare land and road objects, where the remarkable changes are the alterations of land cover. The corresponding images are shown in Fig. 3(a) and (b). The second data set (DS2) contained Gaofen 1 (GF-1) images, generated by fusing panchromatic and multispectral images, comprised of four bands of red, green, blue, and near infrared with a spatial resolution of 2 m. These images were acquired over Beijing, China in November 2014 and again in January 2016. The region is a 1455 × 1109 pixels area containing buildings, vegetation, bare land, field land, and water areas. The main changes are the buildings and water areas, which are illustrated in Fig. 3(d) and (e). All the data sets were automatically coregistered with an RMSE of registration less than 0.5 pixels. The relative radiometric correction was implemented by applying the pseudo-invariant feature (PIF) method.

For each testing data set, a reference change map was prepared for qualitative evaluation purposes, which was manually generated according to a detailed visual interpretation, as shown in Fig. 3(c) and (f). Four metrics were used to permit a quantitative evaluation of the CD results: 1) the false alarm (FA) rate, which is the number of unchanged pixels incorrectly detected as changed pixels over the total number of unchanged pixels; 2) the missed detection (MD) rate, which is the number of changed pixels detected as unchanged pixels over the total number of changed pixels; 3) the overall accuracy (OA), which is the total number of correctly detected pixels over the total number of pixels; and 4) the kappa coefficient.

To demonstrate the performance of the proposed approach, three state-of-the-art methods were implemented for comparisons: EM [3], PCA and k-means clustering (PCAK) [7], and OBCD using multi-scale fusion (OB-MSF) [18]. In the two experiments conducted, the relevant parameters were set as follows. In multiscale segmentation, the shape and compactness weights were set at 0.2 and 0.7 based on experiences, and the optimal scales, s, were determined using the GS method, where $s = \{40, 80, 120\}$ in DS1 and $s = \{30, 60, 100\}$ in DS2.

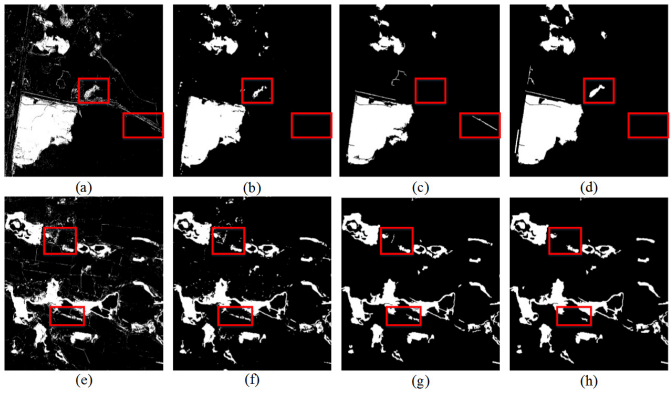

Fig. 4. CD results of two data sets. CD results obtained by (a) EM, (b) PCAK, (c) OB-MSF, and (d) OB-MSUA in DS1. CD results obtained by (e) EM, (f) PCAK, (g) OB-MSF, and (h) OB-MSUA in DS2.

The threshold for uncertainty analysis was set at 0.75, which proved to perform best. In SVM, the RBF kernel was selected, and the two parameters, C and γ, were adaptively selected according to the 2-D grid searching strategy.

B. Results and Analysis

The CD results of the different approaches on two data sets are shown in Fig. 4. Visual comparisons of the results of the four CD methods generally indicate their performance. The EM-based method [Fig. 4(a) and (e)] performed poorly on both DS1 and DS2, because the contextual information is neglected and "salt and pepper" noise arise, which can seriously affect CD accuracy. PCAK [Fig. 4(b) and (f)] performed much better than EM, which mainly lies in the usage of contextual information by neighboring windows. Compared with EM and PCAK, OB-MSF [Fig. 4(c) and (g)] and OB-MSUA [Fig. 4(d) and (h)] removed the "salt and pepper" noise and achieved better visual performance, due to their usage of segmented objects as the basic analysis unit. In OB-MSF, the CD results from different scales were treated independently and then combined using adaptive weights, which neglects the scale constraints between scales. Contrary to OB-MSF, the scale constraints were considered by OB-MSUA, where fewer false alarms and miss detections occurred on both data sets. Fig. 5 displays the multi-scale uncertainty analysis process of OB-MSUA on DS1 and DS2, where the red, black and yellow areas denote the changed, unchanged, and uncertain class respectively. Many yellow areas can be seen in the coarse-scale CD results [Fig. 5(a) and (d)], but there are less in the finer scale CD results [Fig. 5(b) and (e)], which indicates that the uncertain information was refined after projecting it onto the finer scales and implementing the uncertainty analysis. The remained uncertain information was further refined in the next-finer scales [Fig. 5(c) and (f)].

Table I reports the quantitative evaluations results of the different CD methods, from which it was concluded that the OBCD methods (OB-MSF and OB-MSUA) performed better than the PBCD methods (EM and PCAK). Furthermore, the proposed OB-MSUA method was superior to all the other methods in terms of OA and kappa coefficient for both data sets. Specifically, in DS1, the OA for OB-MSUA were improved by 1.74%, 0.66%, and 0.71% over EM, PCAK and OB-MSF respectively, and the kappa coefficient was improved by 0.065, 0.030 and 0.031, respectively. In DS2, the OA for OB-MSUA were improved by 3.17%, 1.52%,

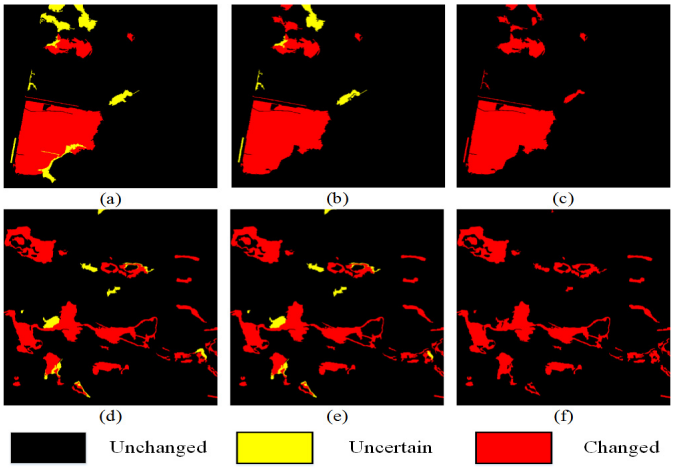

Fig. 5. CD results from different scales. CD result from scales (a) 120, (b) 80, and (c) 40 in DS1. CD result from scales (d) 100, (e) 60, and (f) 30 in DS2.

TABLE I

SUMMARY OF THE QUANTITATIVE EVALUATIONS FOR DIFFERENT METHODS ON DS1 AND DS2

Dataset	Method	MD (%)	FA (%)	OA (%)	Kappa
DS1	EM	2.54	13.46	95.85	0.8359
	PCAK	3.17	2.36	96.93	0.8704
	OB-MSF	3.09	3.31	96.88	0.8691
	OB-MSUA	**2.34**	**2.89**	**97.59**	**0.9006**
DS2	EM	2.22	27.87	94.30	0.7420
	PCAK	2.32	17.15	95.95	0.8036
	OB-MSF	2.21	8.50	97.12	0.8551
	OB-MSUA	**1.97**	**7.13**	**97.47**	**0.8731**

and 0.35% over EM, PCAK, and OB-MSF respectively; and the kappa coefficient was improved by 0.130, 0.070 and 0.018 respectively. There are two reasons for these noticeable improvements. In the PBCD methods such as EM and PCAK, contextual information is better considered and CD accuracy thus increased; and when compared with OB-MSF, the scale constraints are fully considered by implementing the multiscale uncertainty analysis, through which uncertain information is reduced layer by layer.

IV. CONCLUSION

A novel OBCD technique, which is capable of delineating and analyzing image ground objects from different scales based on multi-scale uncertainty analysis (OB-MUSA), was proposed and successfully implemented for VHR images in this letter. OB-MUSA first stacks and segments two temporal images using a series of predefined optimal scales ranging from coarse to fine, from which the initial CD results are generated by searching the PBCD and OBCD results using D-S evidence theory. The uncertain information in the initial CD results then are further refined after projecting them onto the finer scales and implementing the uncertainty analysis using SVM. Finally, the CD map is generated by combining all the certain change maps from different scales. The effectiveness and reliability of OB-MUSA were evaluated using SPOT5 and GF-1 images, and the results confirmed that OB-MUSA has the ability to achieve better CD results for VHR images than some of the state-of-the-art methods. Future work will focus on the automatic segmentation and parameter selection process to further improve the CD performance.

REFERENCES

[1] A. Singh, "Review article digital change detection techniques using remotely-sensed data," *Int. J. Remote Sens.*, vol. 10, no. 6, pp. 989–1003, 2010.
[2] M. Hussain, D. Chen, A. Cheng, H. Wei, and D. Stanley, "Change detection from remotely sensed images: From pixel-based to object-based approaches," *ISPRS J. Photogramm. Remote Sens.*, vol. 80, no. 2, pp. 91–106, 2013.
[3] L. Bruzzone and D. F. Prieto, "Automatic analysis of the difference image for unsupervised change detection," *IEEE Trans. Geosci. Remote Sens.*, vol. 38, no. 3, pp. 1171–1182, May 2000.
[4] J. S. Deng, K. Wang, Y. H. Deng, and G. J. Qi, "PCA-based land-use change detection and analysis using multitemporal and multisensor satellite data," *Int. J. Remote Sens.*, vol. 29, no. 16, pp. 4823–4838, 2008.
[5] S. Ghosh, M. Roy, and A. Ghosh, "Semi-supervised change detection using modified self-organizing feature map neural network," *Appl. Soft Comput.*, vol. 15, nos. 3–4, pp. 1–20, 2014.
[6] C. Huang *et al.*, "Use of a dark object concept and support vector machines to automate forest cover change analysis," *Remote Sens. Environ.*, vol. 112, no. 3, pp. 970–985, 2008.
[7] T. Celik, "Unsupervised change detection in satellite images using principal component analysis and k-means clustering," *IEEE Geosci. Remote Sens. Lett.*, vol. 6, no. 4, pp. 772–776, Oct. 2009.
[8] Y. Bazi, F. Melgani, and H. D. Al-Sharari, "Unsupervised change detection in multispectral remotely sensed imagery with level set methods," *IEEE Trans. Geosci. Remote Sens.*, vol. 48, no. 8, pp. 3178–3187, Aug. 2010.
[9] P. Jian, K. Chen, and C. Zhang, "A hypergraph-based context-sensitive representation technique for VHR remote-sensing image change detection," *Int. J. Remote Sens.*, vol. 37, no. 8, pp. 1814–1825, 2016.
[10] G. Cao, L. Zhou, and Y. Li, "A new change-detection method in high-resolution remote sensing images based on a conditional random field model," *Int. J. Remote Sens.*, vol. 37, no. 5, pp. 1173–1189, 2016.
[11] G. Chen, G. J. Hay, L. M. T. Carvalho, and M. A. Wulder, "Object-based change detection," *Int. J. Remote Sens.*, vol. 33, no. 14, pp. 4434–4457, 2012.
[12] B. Wang, S. Choi, Y. Byun, S. Lee, and J. Choi, "Object-based change detection of very high resolution satellite imagery using the cross-sharpening of multitemporal data," *IEEE Geosci. Remote Sens. Lett.*, vol. 12, no. 5, pp. 1151–1155, May 2015.
[13] Q. Chen and Y. Chen, "Multi-feature object-based change detection using self-adaptive weight change vector analysis," *Remote Sens.*, vol. 8, no. 7, p. 549, 2016.
[14] O. Yousif and Y. Ban, "A novel approach for object-based change image generation using multitemporal high-resolution SAR images," *Int. J. Remote Sens.*, vol. 38, no. 7, pp. 1765–1787, 2017.
[15] C. Wu, L. Zhang, and L. Zhang, "A scene change detection framework for multi-temporal very high resolution remote sensing images," *Signal Process.*, vol. 124, pp. 184–197, Jul. 2016.
[16] R. Qin, X. Huang, A. Gruen, and G. Schmitt, "Object-based 3-D building change detection on multitemporal stereo images," *IEEE J. Sel. Topics Appl. Earth Observ. Remote Sens.*, vol. 8, no. 5, pp. 2125–2137, May 2015.
[17] F. Bovolo, "A multilevel parcel-based approach to change detection in very high resolution multitemporal images," *IEEE Geosci. Remote Sens. Lett.*, vol. 6, no. 1, pp. 33–37, Jan. 2009.
[18] W.-J. Wang, Z.-M. Zhao, and H.-Q. Zhu, "Object-oriented change detection method based on multi-scale and multi-feature fusion," in *Proc. Urban Remote Sens. Event*, 2009, pp. 1–5.
[19] W. Feng and Y. Zhang, "Object-oriented change detection for remote sensing images based on multi-scale fusion," *Acta Geodaetica Cartographica Sinica*, vol. 44, no. 10, pp. 1142–1151, 2015.
[20] M. Baatz and A. Schäpe, "An optimization approach for high quality multi-scale image segmentation," in *Proc. Beiträge AGIT-Symp.*, 2000, pp. 12–23.
[21] B. Johnson and Z. Xie, "Unsupervised image segmentation evaluation and refinement using a multi-scale approach," *ISPRS J. Photogramm. Remote Sens.*, vol. 66, no. 4, pp. 473–483, Jul. 2011.
[22] D. Peng and Y. Zhang, "Object-based change detection from satellite imagery by segmentation optimization and multi-features fusion," *Int. J. Remote Sens.*, vol. 38, no. 13, pp. 3886–3905, 2017.
[23] J. C. Bezdek, R. Ehrlich, and W. Full, "FCM: The fuzzy c-means clustering algorithm," *Comput. Geosci.*, vol. 10, nos. 2–3, pp. 191–203, 1984.
[24] J. Inglis, "A mathematical theory of evidence," *Technometrics*, vol. 20, no. 1, p. 242, 1976.